

The K -band luminosity function of nearby field galaxies

Jon Loveday

Department of Astronomy and Astrophysics, University of Chicago, 5640 S. Ellis Ave, Chicago, IL 60637, USA
loveday@oddjob.uchicago.edu

9 March 2022

ABSTRACT

We present a measurement of the K -band luminosity function (LF) of field galaxies obtained from near-infrared imaging of a sample of 345 galaxies selected from the Stromlo-APM Redshift Survey. The LF is reasonably well-fit over the ten magnitude range $-26 \leq M_K \leq -16$ by a Schechter function with parameters $\alpha = -1.16 \pm 0.19$, $M^* = -23.58 \pm 0.42$, $\phi^* = 0.012 \pm 0.008 \text{ Mpc}^{-3}$, assuming a Hubble constant of $H_0 = 100 \text{ km s}^{-1} \text{Mpc}^{-1}$. We have also estimated the LF for two subsets of galaxies subdivided by the equivalent width of the $\text{H}\alpha$ emission line at $\text{EW}(\text{H}\alpha) = 10 \text{\AA}$. There is no significant difference in LF shape between the two samples, although there is a hint ($\sim 1\sigma$ significance) that emission line galaxies (ELGs) have M^* roughly one magnitude fainter than non-ELGs. Contrary to the optical LF, there is no difference in faint-end slope α between the two samples.

Key words: cosmology: observations — galaxies: luminosity function, mass function — surveys

1 INTRODUCTION

Deep, near-infrared K -band ($2.2\mu\text{m}$) galaxy surveys are a powerful tool for studying galaxy evolution, eg. Gardner, Cowie & Wainscoat (1993), Cowie et al. (1994), Glazebrook et al. (1995). Compared to blue-optical light, near-infrared light is a better tracer of mass in evolved stars and the correction for redshift dimming (the “ k -correction”) is approximately independent of morphological type. The rapid evolution in galaxy number counts apparent in the b_J band is not seen in the K band, eg. Koo & Kron (1992). However, it is vital to have a reliable determination of the K -band luminosity function (LF) for *nearby* galaxies in order to interpret faint galaxy counts and to calculate the clustering of K -selected galaxy samples. Local K -band luminosity functions have been measured from optically-selected samples by Mobasher, Sharples & Ellis (1993) and Szokoly et al. (1998) and from K -selected samples by Glazebrook et al. (1995) and Gardner et al. (1997). Since all of these surveys are flux-limited, the majority of galaxies have K -band luminosities close to L_K^* . Even in the largest sample (Gardner et al., 510 galaxies), it was feasible to measure the LF over a range of only 5 magnitudes, M_{-2}^{*+3} , and so the faint-end slope of the K -band luminosity function, so important for predicting galaxy number counts, is still rather poorly constrained.

In this paper we present a new estimate of the K -band LF over a range of ten magnitudes, M_{-2}^{*+8} , based on a sub-sample of galaxies selected from the Stromlo-APM galaxy survey (Loveday et al. 1996). This survey is an ideal source for estimating the K -band LF since redshifts have already

been measured for 1797 galaxies with $b_J < 17.15$ over a very large volume of space. The solid angle of the survey is 1.3 sr and the median redshift is about 15,300 km/s. The key to measuring the faint-end of the K -band LF without a huge investment of telescope time is to observe galaxies selected by their intrinsic luminosity rather than their apparent flux. One can make use of the fact that near-infrared and optical luminosities are correlated (Mobasher, Ellis & Sharples, 1986; Saracco, Chincarini & Iovino 1996), in order to preferentially select galaxies of high and low luminosity and thus sample the luminosity range more uniformly than a flux-limited sample. One is thus able to measure the luminosity function to fainter luminosities than from a flux-limited sample of similar size. This sampling strategy is described in §2 and the observations and data reduction are discussed in §3. Our method of estimating $\phi(M_K)$ from a b_J -selected sample is given in §4 and we test this method in §5. Our results are presented in §6 and we conclude in §7. For notational convenience, we will denote absolute magnitudes in the K and b_J bands by M_K and M_B respectively. Throughout, we assume a Hubble constant of $H_0 = 100 \text{ km/s/Mpc}$.

2 SAMPLE SELECTION

The aim in selecting a subset of Stromlo-APM galaxies for which to obtain K -band photometry was to sample the magnitude range $-22 \leq M_B \leq -13$ (the full range of b_J absolute magnitudes in the Stromlo-APM survey) as uniformly as possible. An added complication in defining the sample

arose because we wished to obtain optical CCD images for the same sample of galaxies. One planned use of this optical imaging is to measure morphological parameters for a representative sample of galaxies at low redshift in order to compare with HST observations of galaxies at high redshift, $z > 0.4$, (Brinchmann et al. 1998). To obtain comparable linear resolution to the HST data required observing galaxies at $z < 0.04$, assuming ground-based seeing of 1.3 arcsecond. Our primary sample thus consists of galaxies at redshifts $z < 0.04$. We divided the magnitude interval $-22 \leq M_B \leq -13$ into 90 bins each of width 0.1 mag. We then randomly selected up to six galaxies from the Stromlo-APM survey with $z < 0.04$ in each bin. Due to the redshift limit of $z < 0.04$, this primary sample contains rather few galaxies brighter than $M_B = -20$. We therefore formed a supplementary sample, consisting of galaxies at $z > 0.04$ to top up each magnitude bin, where possible, to six galaxies. This supplementary sample consists entirely of galaxies with $M_B < -20$. The primary sample contains 283 galaxies, and the supplementary sample contains 80 galaxies, giving a total sample size of 363 galaxies.

3 OBSERVATIONS AND DATA REDUCTION

Imaging of the above sample of galaxies was carried out at the Cerro Tololo Interamerican Observatory (CTIO) 1.5m telescope using the CIRIM infrared array through the standard K filter over the nine nights 1996 August 31 – September 4 and 1997 October 19–22. The pixel size at $f/7.5$ is $1.16''$, allowing most galaxies to be observed at 9 non-overlapping positions on the 256×256 array. Two frames were taken with the galaxy at the central position, thus yielding 10 frames per galaxy. Total integration time for each galaxy was 300 seconds. For 11 galaxies with angular size more than 100 arcsec, we obtained four on-source and four offset-sky integrations of 75 seconds each. In the following, these will be referred to as “biggrid” observations. Standard stars were observed from the list of Elias et al. (1982). Dark frames and dome flats were taken at the start of each night.

The infrared frames were reduced using IRAF, mosaiced with the DIMSUM^{*} package and image detection and photometry was performed using SExtractor (Bertin & Arnouts 1996).

3.1 Basic reduction

The basic reduction process consisted of the following steps:

- (i) Non-linearity correction using the IRLINCOR task with parameters $c1 = 0.9997$, $c2 = 0.0257$, $c3 = 0.0158$ (Mike Keane, private communication),
- (ii) Subtraction of dark frame,
- (iii) Flatfielding by dome flat,
- (iv) Masking of bad pixels.

^{*} DIMSUM is the Deep Infrared Mosaicing Software package developed by Peter Eisenhardt, Mark Dickinson, Adam Stanford, and John Ward, and is available via ftp from <ftp://iraf.noao.edu/iraf/contrib/dimsumV2/dimsum.tar.Z>

3.2 Mosaicing

At this stage of the reduction we had ten frames per galaxy, with the galaxy at a different position on each frame. Mosaicing of the frames and subtraction of sky background was performed using the DIMSUM package. As described by Stanford, Eisenhardt & Dickinson (1995), DIMSUM employs a two-pass procedure in order to mask out faint as well as bright images when constructing the sky background, resulting in a much flatter sky than is obtained from median filtering of the galaxy frames with outlier rejection. Individual galaxy frames were block replicated by a factor of 4 in each dimension, allowing alignment to be performed by integer offsets without interpolation. Co-added images and corresponding exposure weight maps were made by summing the aligned images and were finally block averaged 2×2 in order to economize on disc space.

For the 11 “biggrid” observations, the four offset sky frames were median filtered with outlier rejection in order to estimate the sky background. The sky background was subtracted from each of the four on-source frames, which were then aligned and coadded.

3.3 Image detection and photometry

We used SExtractor 2.0.15 to detect and measure images in the mosaiced frames. For both standard stars and galaxies we used the MAG_BEST estimate of magnitude. This yields a pseudo-total magnitude (Kron 1980) except in crowded fields, when a corrected isophotal magnitude is measured instead. Magnitude errors were estimated by combining in quadrature SExtractor’s estimate of the error from photon statistics and the difference between magnitudes measured using local and global estimates of the sky background. Of the selected sample of 363 galaxies, 351 were observed under photometric conditions and 345 yielded a K -band magnitude with an estimated error of less than 0.1 mag (rms mag error = 0.04 mag).

3.4 Calibration

Since we observed only single band infrared imaging, we used the following simple relation to convert observed magnitudes k to standard CIT (Elias et al. 1982) magnitudes K :

$$K = k + k_0 + k_X X, \quad (1)$$

where k_0 is a zero-point offset, k_X is the extinction coefficient in the K -band and X is the airmass of the observation. We made a total of 74 standard star observations during the runs (an average of 8 per night) and we initially fitted the parameters k_0 and k_X for all standard star observations combined, obtaining $k_0 = 7.588 \pm 0.020$ and $k_X = 0.081 \pm 0.018$ with rms residual magnitude error of 0.018. Six standard star observations with large residuals were omitted from the fitting procedure, three of these were from the night of 1996 August 31, which was partially non-photometric. Holding the zero-point term fixed at $k_0 = 7.588$ we then fitted the extinction coefficient separately for each night, with results shown in Table 1. Galaxy magnitudes were converted to the CIT system using (1) with $k_0 = 7.588$ and k_X coefficients from the Table. Galaxies observed during non-photometric

Table 1. Standard star calibration data.

Night	N_{std}^1	N_{del}^2	k_X^3	rms
1996 Aug 31	11	3	0.105 ± 0.006	0.017
1996 Sep 01	4	1	0.101 ± 0.002	0.003
1996 Sep 02	9	0	0.081 ± 0.004	0.014
1996 Sep 03	9	0	0.082 ± 0.004	0.015
1996 Sep 04	7	0	0.092 ± 0.004	0.011
1997 Oct 19	9	0	0.083 ± 0.003	0.010
1997 Oct 20	7	1	0.067 ± 0.004	0.010
1997 Oct 21	11	1	0.075 ± 0.002	0.007
1997 Oct 22	7	0	0.066 ± 0.005	0.013

¹ Number of standard stars observed.

² Number of outliers deleted.

³ Extinction coefficient in (1).

conditions on the nights of 1996 August 31 and 1997 October 20 were rejected: these cases were obvious from the rapidly varying sky background.

3.5 Photometric repeatability

Thirty-one galaxies, mostly of low K -band surface brightness, were observed on more than one occasion, which allows us to assess the repeatability of our photometry. In these cases, we ran SExtractor on the mosaiced galaxy frames both before and after coadding observations. We obtain final photometry from the coadded frame and use the two individual frames and the coadded frame to estimate the rms error. In four cases, one observation was made using “biggrid”: in these cases we do not coadd the observations and instead use the DIMSUM-reduced observation for the final magnitude and estimated error.

In Figure 1 we plot both our estimated errors and the rms errors between repeated observations as a function of K magnitude and mean surface brightness μ_K . The symbols indicate the rms magnitude error and the length of the line shows the estimated magnitude error from the coadded image. Thus if our estimated errors are a good estimate of the true rms then the lower ends of the error bars should reach zero. In most cases, the rms error is within 2–3 times the estimated error and in a few cases the error is slightly overestimated. The five points with rms > 0.4 all correspond to images which were broken up by SExtractor’s deblender (open symbols). We attempted to sum the flux from the components, but clearly the K magnitude for these objects is accurate to only ~ 0.5 mag. We see that most of the discrepant points are of extremely low surface brightness, $\mu_K \gtrsim 21.5$ mag arcsec $^{-2}$. For unbroken images, all rms errors are less than 0.2 mag and the estimated errors provide a reasonable estimate of the rms. The stars denote objects in which one of the observations used separate sky exposures (“biggrid” observations). For two out of four of these objects, we see an rms magnitude error larger than 0.1 but with a negligible estimated error (from the non-biggrid observation). The reason for this is the poorer sky subtraction of the biggrid observations compared with the DIMSUM reduction of the majority of our observations.

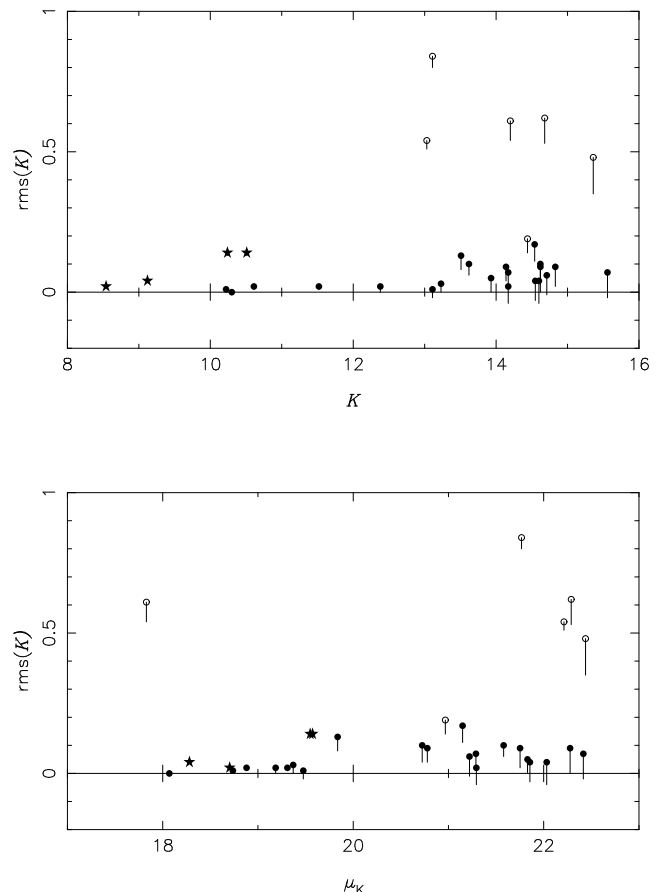


Figure 1. Repeatability of galaxy photometry. The top panel plots the rms K magnitude between repeated observations against K magnitude from the coadded data. The symbols indicate the rms magnitude error and the length of the line shows the estimated magnitude error. The lower panel plots the same information but as a function of mean K -band surface brightness μ_K within the measurement aperture. Open symbols denote sources deblended by SExtractor, stars indicate a “biggrid” observation.

3.6 Matching to APM

Since the mosaiced frames cover an area of sky around 8 arcmin on a side, albeit not to uniform depth, they provide K -band photometry for many objects in each field in addition to the target galaxy. We therefore matched the images detected by SExtractor with images in the APM scans. Using the matched objects in each frame, we calculated a 6-parameter transform from CIRIM pixel coordinates to APM plate coordinates and thence to RA & Dec.

The K -band photometry for the target galaxies is presented in the Appendix to this paper.

3.7 Sample properties

Since our source survey is limited by b_J flux, our K -band sample is not a complete one, as illustrated in Figure 2. At faint K magnitudes, only blue objects will be in the Stromlo-APM sample. We are roughly complete to $K \approx 12$, the bluest galaxies can be seen as faint as $K \approx 15$. The luminosity function estimator described in §4 corrects for this K -band incompleteness and allows us to use all galaxies

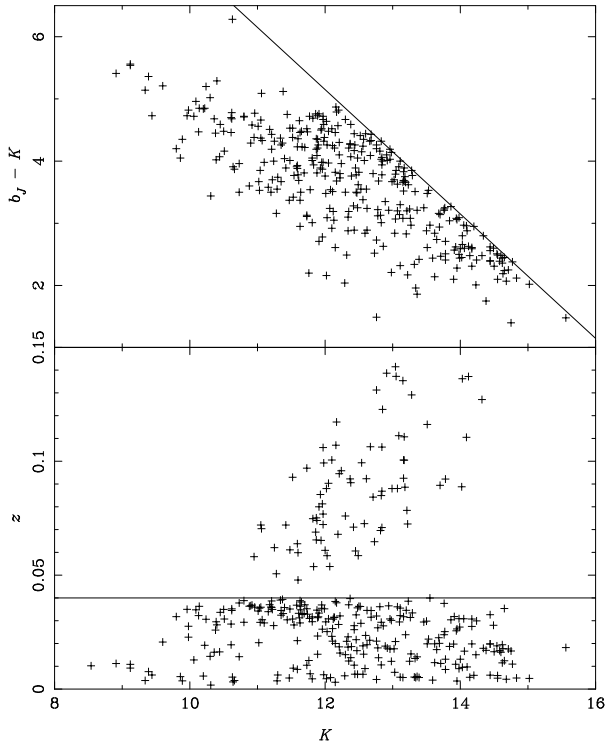


Figure 2. Illustration of observational selection effects in our sample. The upper panel plots observed $b_J - K$ colour versus apparent K magnitude. The line shows the apparent magnitude limit for the Stromlo-APM survey, $b_J = 17.15$. The lower panel plots redshift against apparent K magnitude. The line in this case separates the primary and supplementary samples at $z = 0.04$.

with K -band photometry. In the lower panel of this Figure we plot the redshift distribution as a function of apparent K magnitude. The requirement that $z < 0.04$ for the primary sample has a noticeable effect on the overall redshift distribution: this effect is also accounted for by our luminosity function estimator.

To calculate absolute magnitudes we use galactocentric recession velocities and assume k-corrections in the b_J band as given in Table 2 of Efstathiou, Ellis & Peterson (1988). We assume a K -band k-correction of $-2.5z$ for all galaxy types (ie. the near-infrared k-correction *brightens* galaxies with redshift). This is a very good approximation to the K -band k-correction of Glazebrook et al. (1995) for redshifts $z < 0.15$.

Figure 3 shows the rest-frame ($M_B - M_K$) versus M_K colour-magnitude relation for our data. The fit to all galaxies is given by

$$(M_B - M_K) = -0.212 \times M_K - 1.20, \quad \sigma = 0.77. \quad (2)$$

The slopes in this relation for early and late-type galaxies (-0.135 ± 0.036 and -0.209 ± 0.024 respectively) are consistent with those found for E-S0 (-0.095 ± 0.013) and Sa-Sdm (-0.24 ± 0.03) galaxies by Mobasher, Ellis & Sharples (1986), although we find a significantly larger scatter about the relation. At least part of this scatter is due to saturated APM

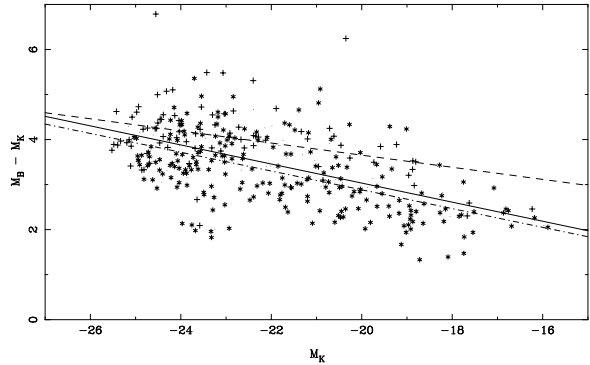


Figure 3. Rest-frame $M_B - M_K$ versus M_K colour-magnitude plot. Plus signs represent early-type galaxies, asterisks late-type galaxies and dots represent unclassified galaxies. The solid line shows a least-squares fit to all galaxies, the dashed line a fit to early types and the dot-dashed line a fit to late type galaxies.

b_J magnitudes for galaxies $b_J \lesssim 15$ and a few instances of the APM scans breaking up a very large, bright galaxy into fragments. An improved colour-magnitude relation will be available when we incorporate optical CCD magnitudes for these galaxies (Loveday & Lilly, in preparation).

4 ESTIMATING THE K -BAND LUMINOSITY FUNCTION

When one has a sample selected on optical b_J magnitude and wishes to estimate the K -band luminosity function, the best way to proceed is to calculate a bivariate luminosity function (BLF, $\phi(M_K, M_B)$) allowing for known selection in b_J flux and M_B absolute magnitude and then to integrate over M_B to obtain $\phi(M_K)$. One can estimate the shape of $\phi(M_K, M_B)$, independently of inhomogeneities in the galaxy distribution, using the maximum likelihood method of Sandage, Tammann & Yahil (1979). The probability of seeing a galaxy with K -band luminosity L_K^i and B band luminosity L_B^i at redshift z_i in our sample is given by

$$p_i = \frac{\phi(L_K^i, L_B^i) S(L_B^i)}{\int_{L_K \min(z_i)}^{L_K \max(z_i)} \int_{L_B \min(z_i)}^{L_B \max(z_i)} \phi(L_K, L_B) S(L_B) dL_K dL_B}. \quad (3)$$

The function $S(L_B)$ accounts for the known selection in absolute B magnitude and the luminosity limits $L_{B,\min}(z_i)$ and $L_{B,\max}(z_i)$ are the minimum and maximum B -band luminosities observable at redshift z_i in a sample limited by apparent b magnitude. For the sample analysed here, there are no flux limits in the k -band, and so the integral over K -band luminosity runs from 0 to $+\infty$. The maximum-likelihood shape of the BLF $\phi(M_K, M_B)$ is estimated by maximizing the likelihood $\mathcal{L} = \prod_{i=1}^{N_g} p_i$ (the product of the individual probabilities p_i for the N_g galaxies in the sample) with respect to the parameters describing the BLF.

In practice, we do not have a good *a priori* parametric model for $\phi(M_K, M_B)$, and so instead we measure $\phi(M_K, M_B)$ in a non-parametric way using an extension

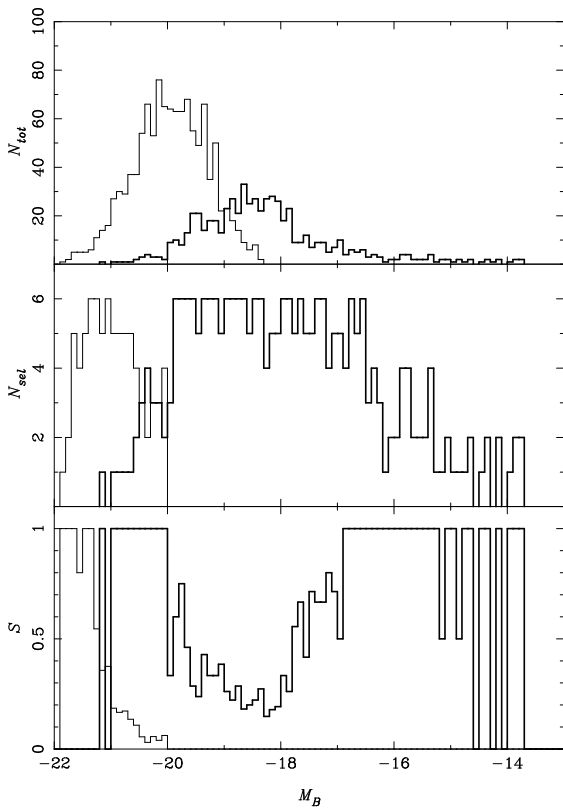


Figure 4. Sample selection as a function of M_B absolute magnitude for the primary (thick lines) and supplementary (thin lines) samples. The upper panel shows histograms of M_B for all 1797 galaxies in the Stromlo-APM survey. The middle panel shows the same for the 345 selected galaxies with K -band photometry. The lower panel shows the sampling functions $S(M_B)$, the ratio of selected to total galaxies in each bin.

of the Efstathiou, Ellis & Peterson (1988) stepwise maximum likelihood (SWML) method. Sodré & Lahav (1993) have extended the SWML method to estimate the bivariate diameter-luminosity function and to allow for sample incompleteness. We adopt their extension of the SWML estimator here, including the sampling function $S(M_B)$ separately for the primary and supplementary galaxy samples. These sampling functions are illustrated in Figure 4, which shows histograms of M_B for the entire Stromlo-APM sample, for the selected galaxies with good K -band photometry and the sampling functions $S(M_B)$.

We measure the bivariate luminosity function in bins of absolute K and B magnitude,

$$\phi(M_K, M_B) = \phi_{jk}, \quad j = 1, \dots, N_{M_K}, \quad k = 1, \dots, N_{M_B}, \quad (4)$$

where $M_K^j - \Delta M_K/2 < M_K < M_K^j + \Delta M_K/2$ and $M_B^k - \Delta M_B/2 < M_B < M_B^k + \Delta M_B/2$.

The log-likelihood is given by

$$\ln \mathcal{L} = \sum_{i=1}^{N_g} \sum_{j=1}^{N_{M_K}} \sum_{k=1}^{N_{M_B}} W_{ijk} \ln[\phi_{jk} S(M_B^k)] -$$

$$\sum_{i=1}^{N_g} \ln \left[\sum_{j=1}^{N_{M_K}} \sum_{k=1}^{N_{M_B}} H_{ijk} \phi_{jk} \right] + \text{const.} \quad (5)$$

Here $W_{ijk} \equiv W(M_K^i - M_K^j, M_B^i - M_B^k)$, with,

$$W(x, y) = \begin{cases} 1 & \text{if } -\Delta M_K/2 \leq x \leq \Delta M_K/2 \\ & \text{and } -\Delta M_B/2 \leq y \leq \Delta M_B/2, \\ 0 & \text{otherwise.} \end{cases} \quad (6)$$

The sampling function $S(M_B)$ (Fig. 4) is incorporated into the ramp function H . Writing $M_K^- = M_K^j - \Delta M_K/2$, $M_K^+ = M_K^j + \Delta M_K/2$, $M_B^- = M_B^k - \Delta M_B/2$, and $M_B^+ = M_B^k + \Delta M_B/2$, then

$$H_{ijk} = \frac{1}{\Delta M_K \Delta M_B} \int_{M_K^-}^{M_K^+} dM_K \int_{M_B^-}^{M_B^+} S(M_B) dM_B, \quad (7)$$

where $M_K' = \max[M_K^-, \min(M_K^+, M_K^{\lim})]$ and $M_B' = \max[M_B^-, \min(M_B^+, M_B^{\lim})]$.

To fix the otherwise arbitrary normalisation constant we apply the constraint

$$g = \sum_j \sum_k \phi_{jk} \left(\frac{L_K}{L_f} \frac{L_B}{L_f} \right)^\beta \Delta M_K \Delta M_B - 1 = 0 \quad (8)$$

with $\beta = 1.5$ and the fiducial luminosity L_f corresponding to $M = -20$ using a Lagrangian multiplier λ . The new likelihood $\ln \mathcal{L}' = \ln \mathcal{L} + \lambda g$ is maximised with respect to the ϕ_{jk} and λ , requiring that $\lambda = 0$.

Setting $\partial \ln \mathcal{L}' / \partial \phi_{jk} = 0$, one arrives at a maximum likelihood estimate for ϕ_{jk} ,

$$\phi_{jk} = n_{jk} \sqrt{\sum_i^{N_g} \left[\frac{H_{ijk} \Delta M_K \Delta M_B}{\left(\sum_{l=1}^{N_{M_K}} \sum_{m=1}^{N_{M_B}} \phi_{lm} H_{ilm} \Delta M_K \Delta M_B \right)} \right]}, \quad (9)$$

where $n_{jk} = \sum_{i=1}^{N_g} W_{ijk}$ is the number of galaxies in the (j, k) th bin. Errors in ϕ_{jk} are estimated via the inverse of the information matrix (Efstathiou et al. 1988).

As with all density-independent estimators, information about the overall normalisation is lost. We therefore normalise our BLF to the mean density of galaxies with $-22 \leq M_B \leq -13$ in the full Stromlo-APM sample, $\bar{n} = 0.071 h^3 \text{Mpc}^{-3}$, calculated as described by Loveday et al. (1992). (Note that the density $\bar{n} = 0.047 h^3 \text{Mpc}^{-3}$ quoted by Loveday et al. (1992) is for the restricted magnitude range $-22 \leq M_B \leq -15$.)

Finally, we obtain the K -band luminosity function by summing over B magnitude bins,

$$\phi(M_K^j) = \sum_{k=1}^{N_{M_B}} \phi_{jk}. \quad (10)$$

One can then fit a given functional form, eg. a Schechter (1976) function, to the stepwise estimate by least-squares.

5 TEST OF THE METHOD

We have tested the above procedure by using it to estimate the K -band luminosity function from a set of Monte Carlo simulations. We generated nine mock Stromlo surveys by a Soneira & Peebles (1978) hierarchical clustering simulation

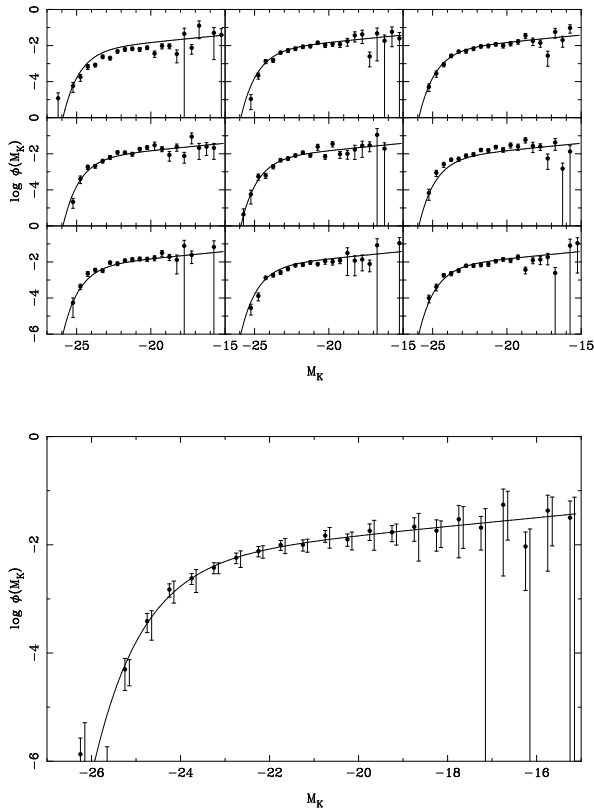


Figure 5. Test of our method to estimate the K -band luminosity function from b_J -limited samples. The upper panels show the K -band LF estimated from each of nine Soneira-Peebles simulations and the lower panel shows the mean and rms (error bars offset to right). In each case the curve shows the *input* LF.

with similar clustering properties to that measured from the Stromlo-APM Survey (Loveday et al. 1995). Each galaxy in the simulation was assigned a K -band luminosity drawn at random from a Schechter function with $\alpha = -1.20$ and $M_K^* = -23.6$ and then assigned a b_J magnitude according to our observed colour-luminosity relation (2). Galaxies were selected on their apparent b_J magnitude, $b_J < 17.15$. This process was repeated until each simulation contained 2000 galaxies. We then sampled each simulation by absolute M_B magnitude as described in §2, finally yielding an average of 359 galaxies per simulation. We calculated the K -band luminosity function $\phi(M_K)$ for each simulation as described in §4 and fit a Schechter function to each by least squares. Averaging over the nine simulations, and estimating the BLF in bins of width 0.5 mag, we measure mean and rms Schechter function parameters $\alpha = -1.17 \pm 0.07$, $M^* = -23.6 \pm 0.2$. The errors on the mean values are $\sqrt{9}$ times smaller than the quoted rms scatter between the simulations. Our estimates of α and M^* are in excellent agreement with the input luminosity function.

The SWML estimates of the K -band LF for the simulations are shown in Figure 5. The points show the SWML estimate of $\phi(M_K)$ from the nine simulations and the curve shows the input Schechter function with shape $\alpha = -1.20$, $M_K^* = -23.6$. The error bars going through the data points show the errors determined from the covariance matrix. The

lower panel shows the average over the 9 simulations. The rms scatter between realisations for each data point (shown by the error bars offset slightly to the right) are in satisfactory agreement with the predicted errors.

Overall, we find that our procedure for estimating $\phi(M_K)$ from a sample limited by apparent b magnitude and further selected by absolute B magnitude provides a robust and unbiased estimate of the K -band LF over a wide range of absolute magnitudes.

6 RESULTS

Our estimated K -band luminosity function is shown in Figure 6. The curve shows a Schechter function fit to the SWML estimate using least squares. We allow for finite bin width by calculating the mean predicted $\langle \phi_j \rangle$ at the absolute magnitude of each galaxy in each bin, rather than simply calculating $\phi(M)$ at the bin centre. The inset shows 1 and 2σ likelihood contours for the shape parameters α and M_K^* , where the normalisation ϕ^* is adjusted to maximize the likelihood at each grid point. The best-fit Schechter parameters are $\alpha = -1.16 \pm 0.19$, $M_K^* = -23.58 \pm 0.42$ and $\phi^* = 0.0121 \pm 0.0082 h^3 \text{Mpc}^{-3}$. The quoted errors on α and M_K^* come from the bounding-box of the 1σ likelihood contour.

Clearly the characteristic magnitude M_K^* is rather poorly constrained from these data, and so in order to measure the faint-end slope α independent of M_K^* , we have also fit a straight line to our estimated LF over the restricted luminosity range $M > -22$. We measure a slope -1.08 ± 0.15 , consistent with that measured from the Schechter fit. Furthermore, this slope does not change significantly varying the bright luminosity cut from -20.5 to -23 .

Since we normalised the LF to the same number density as the full Stromlo-APM sample, the error in ϕ^* is dominated by the uncertainty in shape of the LF. The Schechter function provides a reasonable fit to the SWML estimate over the full range of ten magnitudes; there is no indication of any faint-end turnup.

In Figure 7 and Table 2, we compare our new estimate of the K -band luminosity function with those of other workers. Following Glazebrook et al. (1995) and Gardner et al. (1997), we have added 0.22 mag to the points from Figure 2 of Mobasher et al. (1993) to account for their method of calculating K-corrections. We have also applied an aperture correction of -0.30 mag to the Glazebrook et al. data (see Gardner et al. 1997). Ours is the first estimate of $\phi(M_K)$ fainter than $M_K = -20$. Brighter than this all estimates are in reasonable agreement, particularly given the uncertainties in the normalisation of the LF from small samples of galaxies. The normalisation of the Glazebrook et al. (1995) sample is about twice that of all the other samples. This is likely to be due to sampling fluctuations, since their survey covers only 552 arcmin² and contains a total of only 124 galaxies.

Note that the bright-end points of our estimated LF have dropped significantly since the preliminary analysis of Loveday (1998). This is largely due to the improved K -band photometry obtained by mosaicing the galaxy frames with DIMSUM compared with a cruder algorithm used earlier.

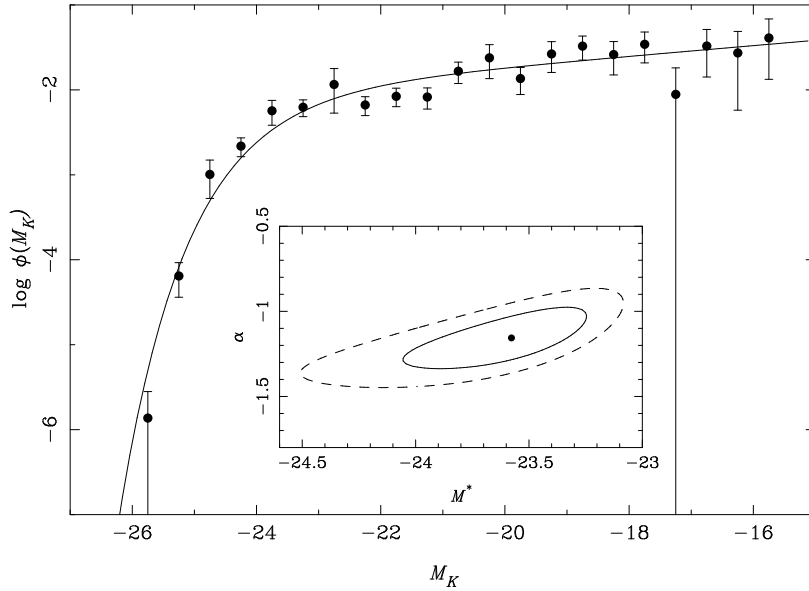


Figure 6. The K -band luminosity function estimated from our sample (symbols) together with the best-fit Schechter function. The inset shows the 1 and 2 σ likelihood contours for the shape parameters α and M_K^* .

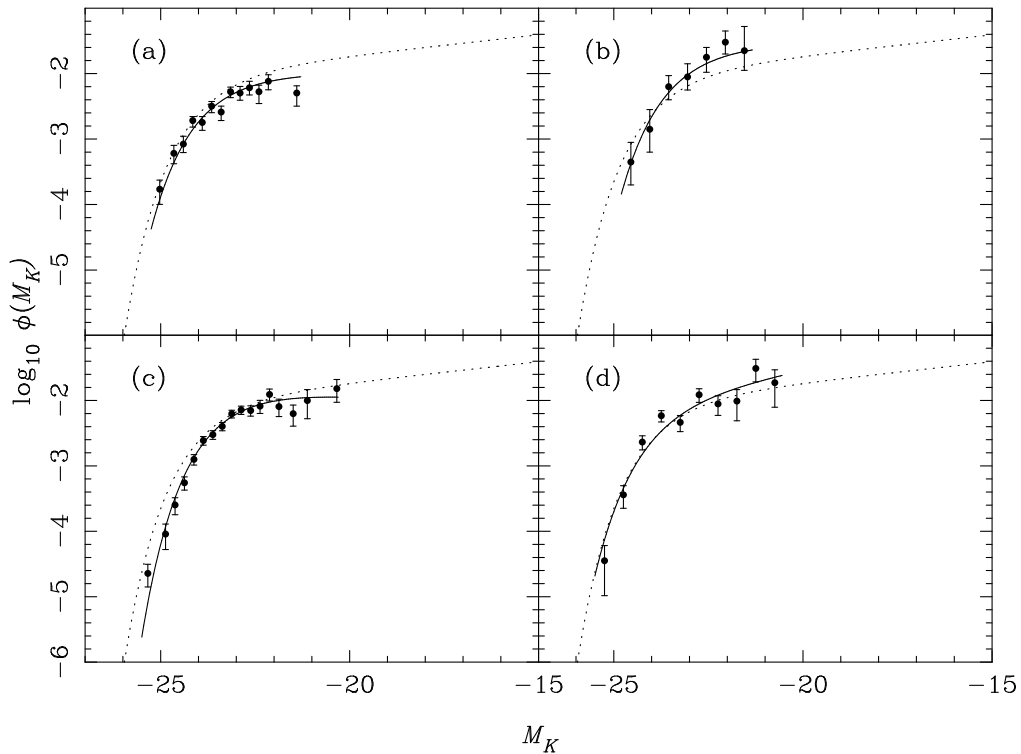
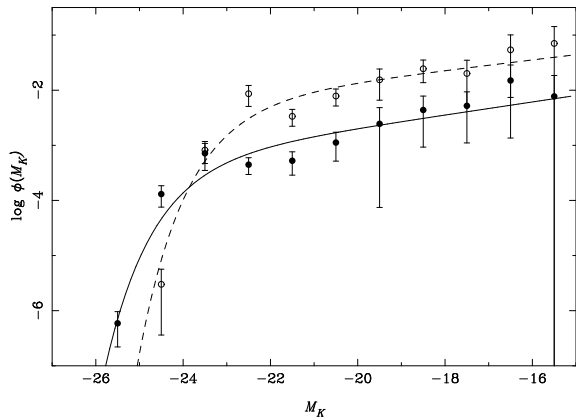


Figure 7. Comparison of our new estimate of the K -band luminosity function (dotted line) with estimates from (a) Mobasher et al., (b) Glazebrook et al., (c) Gardner et al. and (d) Szokoly et al.

Table 2. Schechter function fits to K -band LFs.

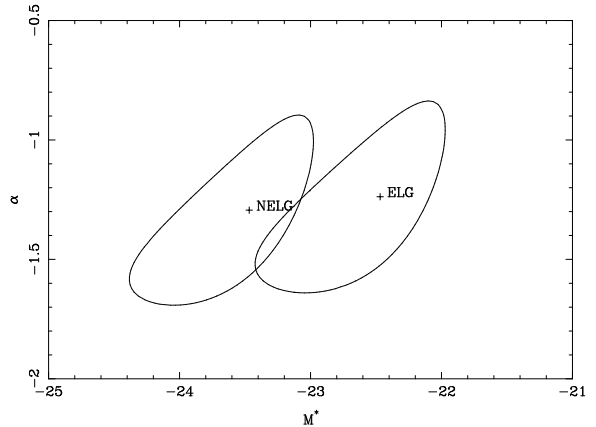
Sample	α	M_K^*	$\phi^*/h^{-3}\text{Mpc}^3$
Mobasher et al. 1993	-1.0 ± 0.3	-23.4 ± 0.3	0.0112 ± 0.0016
Glazebrook et al. 1995 ($z < 0.2$)	-1.04 ± 0.31	-23.02 ± 0.23	0.029 ± 0.007
Gardner et al. 1997	-0.91 ± 0.24	-23.12 ± 0.17	0.0166
Szokoly et al. 1998	-1.3 ± 0.2	-23.6 ± 0.3	0.012 ± 0.004
This work (all galaxies)	-1.16 ± 0.19	-23.58 ± 0.42	0.012 ± 0.008
This work (non-ELG)	-1.3 ± 0.4	-23.5 ± 0.7	0.001 ± 0.001
This work (ELG)	-1.2 ± 0.4	-22.5 ± 0.8	0.011 ± 0.013

**Figure 8.** Comparison of the K -band luminosity function estimated from our non-ELG sample (filled symbols, continuous line) and ELG sample (open symbols, dashed line).

6.1 ELG versus non-ELG

As an aid to understanding the processes of galaxy formation and evolution, it is of great help to have estimates of the luminosity function for different types of galaxies. The most objective way of separating Stromlo-APM galaxies is via the equivalent width of the $\text{H}\alpha$ emission line (Loveday, Tresse & Maddox 1999, hereafter LTM). Due to the small size of our K -band sample, we subdivide into just two subsamples, those with $\text{EW}(\text{H}\alpha) < 10\text{\AA}$ (non-ELG, 138 galaxies) and those with $\text{EW}(\text{H}\alpha) \geq 10\text{\AA}$ (ELG, 134 galaxies). For the remaining 71 galaxies, no $\text{EW}(\text{H}\alpha)$ measurement is available (LTM). For both subsamples we recalculated the sampling function $S(M_B)$ appropriate for galaxies with $\text{EW}(\text{H}\alpha)$ less or greater than 10\AA as appropriate. The LFs were normalised to mean densities of $\bar{n} = 0.018 h^3\text{Mpc}^{-3}$ (non-ELG) and $\bar{n} = 0.098 h^3\text{Mpc}^{-3}$ (ELG) as determined for galaxies with these emission line properties from the full Stromlo-APM sample. The fact that the estimated mean density of ELGs is larger than that for galaxies of any $\text{EW}(\text{H}\alpha)$ ($\bar{n} = 0.071 h^3\text{Mpc}^{-3}$, cf. §4) is a consequence of the mean density of subsamples of Stromlo-APM galaxies being determined to only $\sim 30\%$ accuracy (LTM).

The estimated LFs for each subsample are shown in Figure 8 and the 1σ likelihood contours for the best fit Schechter parameters are shown in Figure 9. The Schechter function parameters themselves are listed in Table 2. Compared with the optical luminosity functions for $\text{EW}(\text{H}\alpha)$ -selected samples (LTM), the K -band LFs for ELGs and non-ELGs are very similar in shape, with just a $\sim 1\sigma$ indication that ELGs

**Figure 9.** 1σ likelihood contours for the best fit Schechter parameters for the non-ELG and ELG samples.

have characteristic magnitudes M^* about one magnitude fainter than non-ELGs. Note that the faint-end slopes for the two samples are completely consistent. These results are in accord with the LFs estimated for E/S0 and spiral galaxies by Mobasher et al. (1993).

7 CONCLUSIONS

We have presented a new estimate of the K -band luminosity function obtained from infrared array imaging of a subsample of galaxies from the Stromlo-APM survey. We measure $\phi(M_K)$ over a range of 10 magnitudes, $M_K^* + 8$, a significantly greater range of luminosities than has been measured before now. Our LF is consistent with earlier estimates, and shows that a Schechter function of moderate faint-end slope ($\alpha = -1.16$) provides a good fit to the LF as faint as $M_K^* + 8$ with no hint of any upturn at the faint-end. This observation appears to rule out the suggestion of Glazebrook et al. (1995) that there may be an extra dwarf component to the K -band LF, or at least that if there is such a component, it must have characteristic magnitude $M_{\text{dwarf}} \gtrsim M_K^* + 8$. In contrast, the faint-end upturn seen in the field b_J LF (Loveday 1997) is apparent by $M_B^* + 6$, and in the CfA Redshift Survey (Marzke, Huchra & Geller 1994) by $M_{Zw}^* + 3$. In the Coma cluster, an upturn in the H -band ($1.6\mu\text{m}$) LF is also seen at $M_H^* + 3$ (De Propris et al. 1998). Note that we do see a slight upturn in $\phi(M_K)$ near $M_K^* + 3$, faintward of the three low points around $M_K = -22$, but the LF flattens out again by $M_K = -20$.

The K -band LFs for non-ELGs and ELGs are very sim-

ilar in shape, with no difference in faint-end slopes, contrary to what is seen in the optical LF (LTM). The steep optical LF for ELGs might be consistent with a \sim flat mass function in a fading burst model (Hogg & Phinney 1997), although the particular model that Hogg & Phinney consider would steepen the K -band LF even more than the optical LF.

The main limitation with our sample is that the b_J selection of the source survey introduces a bias against red galaxies compared to a K -selected sample. However, the good agreement between the K -band LFs determined from K and b_J -limited samples in Fig. 7 suggests that our b_J selection does not significantly affect the estimated K -band LF. In particular, it is unlikely that we are underestimating the faint-end slope of the K -band LF since red galaxies tend to be luminous in K (Mobasher, Ellis & Sharples, 1986; Saracco, Chincarini & Iovino 1996). We will further address the issue of colour selection in a future paper in which we plan to parameterize the bivariate LF $\phi(M_K, M_B)$ using CCD b_J magnitudes in addition to the K -band data presented here.

ACKNOWLEDGMENTS

It is a pleasure to thank George Efstathiou for suggesting this project, the CTIO staff for their excellent support, and Bahram Mobasher, Jon Gardner, Karl Glazebrook and Gyula Szokoly for sending me their K -band LF data points.

REFERENCES

Bertin, E. & Arnouts, S., 1996, A&AS, 117, 393
 Brinchmann, J., et al., 1998, ApJ, 499, 112
 Cowie, L.L., Gardner, J.P., Hu, E.M., Songaila, A., Hodapp, K.-W., & Wainscoat, R.J., 1994, ApJ, 434, 114
 De Propris, R., Eisenhardt, P.R., Stanford, S.A. & Dickinson, M., 1998, ApJ, 503, L45
 Efstathiou, G., Ellis, R.S. & Peterson, B.A., 1988, MNRAS, 232, 431
 Elias, J. H., Frogel, J. A., Matthews, K., & Neugebauer, G., 1982, AJ, 87, 1029
 Gardner, J.P., Cowie, L.L. & Wainscoat, R.J., 1993, ApJ, 415, L9
 Gardner, J.P., Sharples, R.M., Frenk, C.S., Carrasco, B.E., 1997, ApJL, 480, 99
 Glazebrook, K., Peacock, J.A., Miller, L. & Collins, C.A., 1995, MNRAS, 275, 169
 Hogg, D.W. & Phinney, E.S., 1997, ApJ, 488, L95
 Koo, D.C. & Kron, R.G., 1992, ARA&A, 30, 613
 Kron, R.G., 1980, ApJS, 43, 305
 Loveday, J., 1996, MNRAS, 278, 1025
 Loveday, J., 1997, ApJ, 489, 29
 Loveday, J., 1998, in Proceedings of IAU colloquium 171, eds. J.I. Davies, C. Impey & S. Phillipps, in press (astro-ph/9810131)
 Loveday, J., Peterson, B.A., Efstathiou, G. & Maddox, S.J., 1992, ApJ, 390, 338
 Loveday, J., Maddox, S.J., Efstathiou, G., & Peterson, B.A., 1995, ApJ, 442, 457
 Loveday, J., Peterson, B.A., Maddox, S.J., & Efstathiou, G., 1996, ApJS, 107, 201
 Loveday, J., Tresse, L., & Maddox, S.J., 1999, MNRAS, in press (LTM)
 Marzke, R.O., Huchra, J.P., & Geller, M.J., 1994, ApJ, 428, 43
 Mobasher, B., Ellis, R.S. & Sharples, R.M., 1986, MNRAS, 223, 560
 Mobasher, B., Sharples, R.M., & Ellis, R.S., 1993, MNRAS, 263, 560
 Sandage, A., Tammann, G.A. & Yahil, A., 1979, ApJ, 232, 352
 Saracco, P., Chincarini, G., Iovino, A., 1996, MNRAS, 283, 865
 Schechter, P.L., 1976, ApJ, 203, 297
 Sodré, L. & Lahav, O., 1993, MNRAS, 260, 285
 Soneira, R.M. & Peebles, P.J.E., 1978, AJ, 83, 845
 Stanford, S.A., Eisenhardt, P.R.M., & Dickinson, M., 1995, ApJ, 450, 512
 Szokoly, G.P., Subbarao, M.U., Connolly, A.J. & Mobasher, B., 1998, ApJ, 492, 452

APPENDIX A: THE K -BAND DATA

In Table A1 we present a sampling of our K -band photometric data. The complete catalogue will be available from the Astronomical Data Centre (<http://adc.gsfc.nasa.gov/>). The first five columns of this table come from the Stromlo-APM survey (Loveday et al. 1996). The subsequent seven columns are derived from the K -band data. Each column in the table is described below.

- (1) Name: Galaxy naming follows the same convention as the APM Bright Galaxy Catalogue (Loveday 1996) and the Stromlo-APM Redshift Survey (Loveday et al. 1996).
- (2), (3) RA, dec: Right ascension (hours, minutes, seconds) and declination (degrees, arcminutes, arcseconds) in 1950 coordinates.
- (4) b_J : b_J magnitude.
- (5) cz : Heliocentric recession velocity in km/s.
- (6), (7) K , K_{err} : K magnitude and its estimated error.
- (8), (9) Maj, Min: Semi-major and minor axes of measurement ellipse in arcseconds.
- (10) PA: Position angle in degrees measured clockwise from south-north line.
- (11) Flags: Flags output by SExtractor (Bertin & Arnouts 1996).
- (12) Notes:
 - 1: Galaxy deblended by SExtractor; flux of components was summed.
 - 2: “Biggrid” observation: photometry may be less reliable than most galaxies.
 - 3: NGC1672: APM deblended this galaxy.
 - 4: Possibly non-photometric.
 - 5: Central galaxy in close group of 3.
 - 6: Double nucleus.

Table A1. *K*-band galaxy photometry.

Name	RA	Dec	b_J	cz	K	K_{err}	Maj	Min	PA	Flags	Notes
075+069-077	21 26 16.37	-68 39 53.3	16.32	11033	12.50	0.02	16	11	46	3	
076-113-015	22 56 20.64	-69 43 06.6	16.48	3813	13.25	0.04	32	14	61	2	
077+055+032	23 11 33.04	-70 38 10.8	17.05	33310	14.09	0.05	13	8	104	3	
077+062-116	23 11 36.12	-67 52 12.9	16.57	29923	11.98	0.02	19	15	172	3	
078-130-118	00 21 06.17	-62 46 46.8	16.52	12128	13.55	0.04	12	7	116	3	1
078+109+066	23 39 46.85	-66 14 01.5	14.62	10150	11.91	0.07	44	20	86	2	2
078+012+091	23 57 37.39	-66 47 31.6	15.42	21754	11.05	0.01	25	23	69	18	
080-018-033	01 31 33.11	-64 28 28.6	17.01	8088	13.95	0.05	16	12	136	0	
080+009+024	01 26 43.01	-65 31 49.0	14.84	1624	11.47	0.01	25	22	12	0	
082+032-078	02 50 37.37	-63 38 30.4	16.68	30356	13.16	0.03	15	7	110	2	
107-092-049	21 31 44.58	-64 06 47.1	16.14	3179	8.54	0.00	86	43	174	48	
107-009+013	21 17 34.35	-65 19 12.8	16.66	5118	14.06	0.07	18	16	175	2	
107-053-114	21 24 40.36	-62 56 09.3	17.09	8507	14.49	0.08	19	8	152	0	
108+093+006	21 43 24.76	-65 10 25.7	16.03	10497	13.20	0.04	18	14	24	0	
108-114+028	22 20 24.21	-65 32 46.0	16.63	6146	13.69	0.05	26	14	89	0	
108-105+055	22 19 19.57	-66 03 24.1	14.56	10779	11.03	0.01	47	21	47	16	
108-083-130	22 13 20.13	-62 38 40.3	16.85	36934	12.85	0.03	14	13	123	0	
109+063+033	22 32 40.84	-65 41 37.3	16.69	21798	11.97	0.02	18	14	130	0	
109+014+028	22 41 34.01	-65 37 16.2	14.84	3269	11.73	0.02	26	25	31	0	
110+020+024	23 24 18.95	-65 32 45.2	15.04	1991	11.30	0.02	82	38	150	18	
111+063-007	23 50 48.93	-59 58 26.5	14.81	3320	13.05	0.54	53	25	31	0	2
111+118+005	23 42 33.53	-60 08 39.0	15.52	3414	14.24	0.24	30	18	73	2	2
111+025+058	23 56 29.36	-61 11 27.6	16.20	28872	12.24	0.02	24	15	179	0	
112+092-034	00 24 46.45	-59 24 30.9	15.97	11668	12.15	0.02	18	12	75	0	
112-083-068	00 50 12.34	-58 47 36.5	16.15	5150	14.75	0.08	13	9	180	0	
112+079+009	00 26 25.33	-60 13 13.5	16.62	4720	11.89	0.02	38	27	3	16	
113+004+088	01 15 15.04	-61 43 42.3	15.31	8591	11.54	0.01	30	11	7	16	
114-031+009	01 58 39.99	-60 14 34.1	17.06	6743	13.53	0.04	16	6	123	0	
114-015+074	01 56 18.04	-61 27 21.5	14.80	7002	9.98	0.01	49	39	108	16	
114-123-003	02 12 22.81	-59 56 14.5	16.35	1471	15.60	0.14	9	5	93	0	
116-048-060	03 17 06.64	-58 58 03.9	16.62	21466	12.84	0.03	11	11	68	0	
116-074+000	03 21 19.26	-60 04 51.6	17.04	5664	15.56	0.09	16	11	85	3	
117+080-131	03 36 49.50	-57 36 19.7	16.02	4952	12.22	0.02	23	9	31	0	
117+097-087	03 34 07.28	-58 24 46.6	16.11	17774	12.49	0.02	16	8	96	0	
118-094-066	04 39 27.28	-58 50 19.6	14.55	1176	10.64	0.01	26	25	36	16	
118-129-038	04 44 42.52	-59 18 46.7	15.19	1278	7.49	0.00	108	54	90	16	3
118-080+121	04 38 41.93	-62 20 35.2	16.76	8488	14.17	0.06	16	9	72	3	1
118-094+123	04 41 03.91	-62 21 21.0	16.00	6157	13.90	0.05	21	18	60	0	
144+044-118	20 47 21.43	-57 52 35.6	15.32	3233	12.43	0.02	21	17	155	2	
144-126-031	21 12 03.18	-59 26 26.9	16.24	9493	11.89	0.02	11	11	144	0	
144+095-133	20 40 26.42	-57 34 32.3	16.93	10964	12.52	0.02	16	10	128	0	
144+091+082	20 39 21.60	-61 34 36.5	15.69	22306	11.88	0.02	22	15	88	2	
145+055+050	21 23 44.04	-61 02 29.3	15.32	4404	10.30	0.01	34	12	82	2	
145-099-026	21 46 53.28	-59 35 26.3	16.36	8053	12.11	0.02	19	14	40	2	
145+035+005	21 26 58.51	-60 13 18.9	15.07	8660	10.61	0.01	43	32	136	18	
147-070+099	22 59 03.11	-61 53 25.3	17.02	7787	13.94	0.05	23	20	85	2	
148+099-068	23 11 40.26	-58 46 11.3	16.55	3376	13.93	0.05	16	8	30	0	
149-013-101	00 01 43.21	-53 11 47.1	14.60	9773	10.13	0.01	32	25	169	16	
149+031+040	23 55 51.03	-55 48 43.0	16.27	9477	11.62	0.01	22	7	9	0	